RSC Chemical Biology

ROYAL SOCIETY OF CHEMISTRY

PAPER

View Article Online
View Journal | View Issue

Cite this: *RSC Chem. Biol.*, 2025, 6, 882

Thiophosphate bioisosteres of inositol hexakisphosphate enhance binding affinity and residence time on bacterial virulence factors†

Rebecca Cummer,[a] Garvit Bhatt,[ab] Lauren M. Finn,[c] Bettina G. Keller,[c] Bhushan Nagar[b] and Bastien Castagner*[a]

Received 24th September 2024,
Accepted 14th March 2025

DOI: 10.1039/d4cb00228h

rsc.li/rsc-chembio

Inositol phosphates are essential for mammalian cell signalling with critical roles in cellular processes. The fully phosphorylated inositol phosphate, *myo*-inositol hexakisphosphate (**IP6**), modulates numerous eukaryotic proteins and bacterial virulence factors. It has been suggested that the high charge density of **IP6** causes restructuring of virulence factors in mammalian cells, activating their enzymatic activity. **IP6** is challenging to study due to its phytase instability and propensity to precipitate. Here we suggest that the thiophosphate bioisostere, *myo*-inositol hexakisthiophosphate (**IT6**), will mitigate these issues, as thiophosphate substitution has been found to be phytase resistant and improve solubility. Assessment of the chemical properties of **IT6** has indeed validated these characteristics. In addition, we performed biophysical characterization of **IT6** binding to the virulence factors *Salmonella enterica* serovar Typhimurium AvrA, *Vibrio parahaemolyticus* VopA, and *Clostridioides difficile* TcdB. Our data show that the higher charge density of **IT6** increased its binding affinity and residence time on the proteins, which improved stabilization of the bound-state. **IT6** is a valuable tool for structural biology research and the described biophysical characteristics of thiophosphate substitution are of value in medicinal chemistry.

Introduction

Inositol phosphates and their lipidated phosphatidyl inositol congeners are important signaling molecules with crucial roles in cellular processes such as calcium release,[1] insulin signaling,[2] and metabolic signaling pathways.[3] Inositol phosphates are either synthesized from a lipidated inositol core or glucose-6-phosphate *via* a network of kinases, phosphatases, and hydrolases that modulate the attachments on the *myo*-inositol core.[3] Inositol phosphates can exist with various degrees of phosphorylation, ranging from 1 to 6 phosphates, with each species having different functions in the cell. The fully phosphorylated *myo*-inositol hexakisphosphate (**IP6**) modulates numerous eukaryotic proteins and bacterial virulence factors from mammalian and plant pathogens. Examples of mammalian virulence factors include: large clostridial toxins,[4,5] multifunctional autoprocessing RTX toxin,[6,7] HIV-1 gag-hexamer,[8] *Legionella pneumophila* effector kinase,[9] and the *Salmonella enterica* serovar Typhimurium type III effector AvrA.[10] The virulence factors enter host cells either *via* toxin generated pores or a type III secretion system. It is only upon entering their target that the host cytosolic **IP6** modulates the target function through allosteric regulation, by promoting protein stabilization due to the high charge density. Therefore, the **IP6** binding event can form a target specific catalytically active enzyme by stabilizing the virulence factor.

The physicochemical properties of **IP6** permit its varied roles in biological processes. **IP6** is densely charged,[11] a strong chelator of divalent cations,[12] and susceptible to hydrolysis. This simultaneously permits the tight regulation of the varied inositol phosphate species while also acting as a source of phosphate energy regulation.[13–15] Consequently, the compound is hydrophilic, susceptible to cation precipitation,[16] and low in abundance due to its high turnover rate,[17] making **IP6** challenging to study. Given the importance of **IP6** in biology, the development of biomimetics that can tune-out these challenging properties are of value as both structural biology tools and as therapeutics.[18,19]

In an effort to synthesize an **IP6** biomimetic that satisfies the aforementioned properties, thiophosphate and sulfate substitutions have been previously exploited.[20,21] Historically,

[a] *Department of Pharmacology and Therapeutics, McGill University, Montréal, Québec, H3G 1Y6, Canada. E-mail: bastien.castagner@mcgill.ca; Fax: +514-398-2045; Tel: +514-398-2181*
[b] *Department of Biochemistry, McGill University, Montréal, Québec H3G 1Y6, Canada*
[c] *Department of Biology, Chemistry, Pharmacy, Freie Universität, Arnimallee 22, 14195, Berlin, Germany*

† Electronic supplementary information (ESI) available. See DOI: https://doi.org/10.1039/d4cb00228h

thiophosphate substitution has been used in nucleotide synthesis and with lower phosphorylated *myo*-inositols to circumvent enzymatic hydrolysis.[22–26] Thiophosphate drug mimetics have also been found to have an improved lipophilicity due to a decreased hydrogen bond basicity (HBB) favoring octanol in log *P* octanol water partition.[27] In high concentrations of divalent cations, like those found in the gastrointestinal (GI) tract, thiophosphate substitution improves compound solubility.[19] These results suggest that a fully thiophosphorylated **IP6** analog would satisfy the physiochemical properties required to make a promising **IP6** biomimetic. In addition, thiophosphate substitution has been found to improve the potency and stability of the target enzyme(s).[19,28,29] Here, we show that *myo*-inositol hexakisthiophosphate (**IT6**), as previously synthesized by Chen *et al.*,[30] is a useful biomimetic of **IP6** with enhanced resistance towards phytase enzymes and solubility in the presence of divalent cations. Notably, **IT6** can stabilize the *Salmonella enterica* serovar Typhimurium effector AvrA and *Vibrio parahaemolyticus* effector VopA more than their natural co-factor, **IP6**, which was attributed to better binding affinity and slower dissociation rate.

Results and discussion

Synthesis and characterization of IT6

The thiophosphorylated **IP6** analog, **IT6**, was synthesized in a two-step process as described previously (Fig. 1).[30] First, *myo*-inositol was thiophosphorylated by a P^{III} method, followed by sulfur oxidation, generating *myo*-inositol hexakis-dibenzylthiophosphate (**IT6-Bn**). Next, the benzyl protected thiophosphate groups were removed with sodium in liquid ammonia and the compound was purified *via* size-exclusion chromatography.

Interestingly, upon purifying **IT6-Bn** we noticed a sizeable decrease in compound polarity compared to the phosphorylated equivalent, *myo*-inositol hexakis-dibenzylphosphate (**IP6-Bn**, Fig. S1A, ESI†). To elaborate on this, we determined the calculated log *P* (clog *P*) of both compounds and confirmed that **IT6-Bn** was more lipophilic than **IP6-Bn** (20.77 *vs.* 10.69, respectively). To explain these differences, we determined the Hückel charge on each element for both compounds (Fig. S1B, ESI†) and the corresponding compound polar surface area (**IP6-Bn** = 286.56 Å^2 *vs.* **IT6-Bn** = 166.14 Å^2). These results corroborate data from Columbus *et al.* that suggests that thiophosphate substitution of aprotically substituted compounds reduces the hydrogen bond basicity (pK_{HB}) value, improving lipophilicity.[27] It should be noted that in respect to **IP6** and **IT6**, this property is not observed as the phosphate and thiophosphate functional groups on **IP6** and **IT6** have different p*K* values, and the lipophilicities of both compounds are pH dependent. For example, **IT6** has a net charge of −12 at pH 7.4, whereas **IP6** has a net charge of −8, making **IT6** less lipophilic than **IP6** at a physiological pH.[19]

Stability of IT6

First, we evaluated whether **IT6** was resistant to enzymatic hydrolysis by a commercial native wheat phytase. Phytases are a class of enzymes that catalyze the hydrolysis of **IP6** into lower phosphorylated *myo*-inositols and inorganic phosphate (Fig. 2B).[31] Dietary wheat phytase is of physiological importance as it significantly contributes to **IP6** dephosphorylation in mammals.[32] To test whether **IT6** was resistant to enzymatic hydrolysis, we quantified the stability of **IP6** and **IT6** in the presence of phytase-4 over 32 h *via* ^{31}P NMR with the internal standard trimethyl phosphate (TMP). ^{31}P NMR revealed that **IT6** remained completely intact over 32 h, whereas **IP6** was hydrolysed within the first hour of phytase exposure (Fig. 2C). The apparent thiophosphate phytase resistance is likely a result of the thiophosphate phosphoryl being less positively charged than on the phosphate, due to the thiophosphate sulfur being

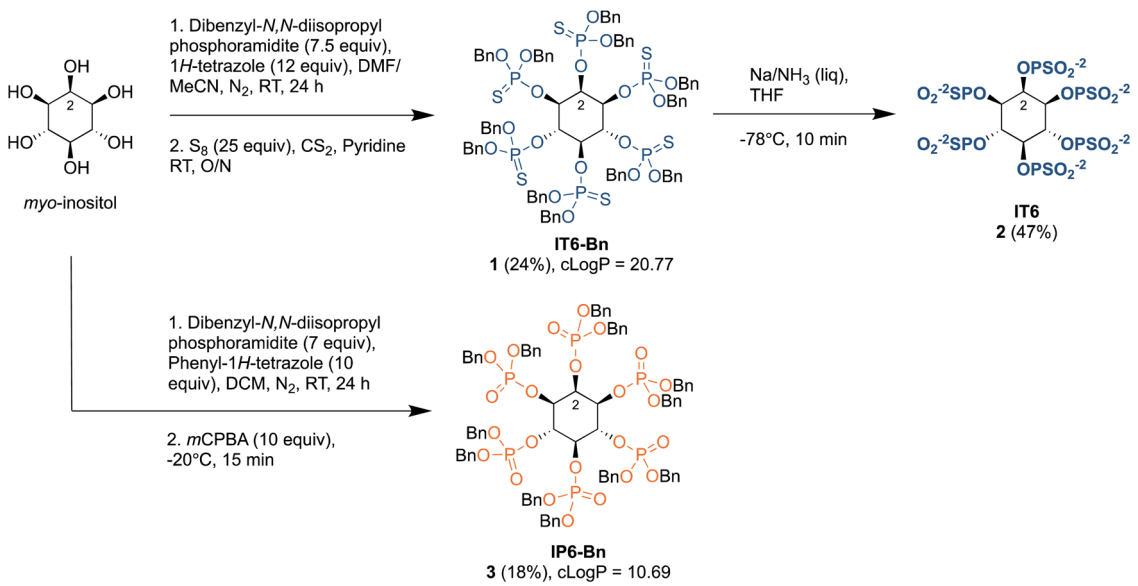

Fig. 1 Scheme of the synthesis of hexakis-thiophosphate (**IT6**)[30] and hexakis-dibenzylphosphate (**IP6-Bn**). *m*CPBA, 3-chloroperbenzoic acid, DCM, dichloromethane; DMF, dimethylformamide; O/N, over night; RT, room temperature; THF, tetrahydrofuran.

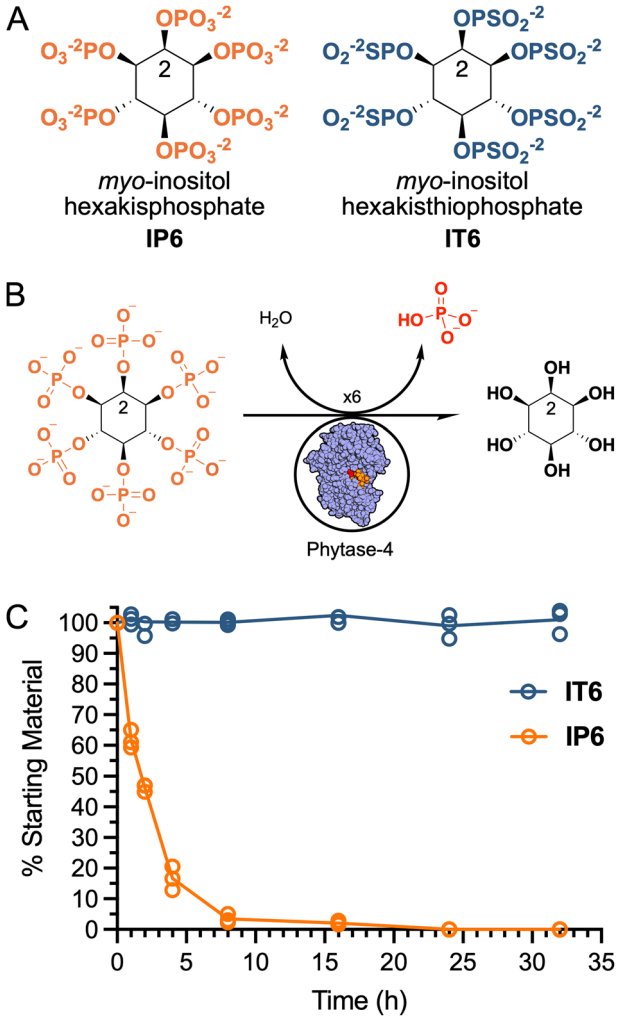

Fig. 2 Stability of **IP6** and **IT6** against phytase-4. (A) Structure of **IP6** and **IT6**. (B) Phytase-4 enzymes remove the phosphate groups from **IP6** *via* hydrolysis (phytase-4 PDB 6GJ2).[31] (C) Percent of 4 mM of **IP6** or **IT6** detectable *via* ^{31}P NMR over 32 h in the presence of phytase-4. n =3 data points are shown.

less electronegative than the oxygen. Since phytase catalysis is initiated by a nucleophilic attack on the phosphorus, the decrease in positive charge reduces the likelihood of said nucleophilic attack. As a result, the thiophosphate esters exhibit greater stability toward neutral and base-catalyzed hydrolysis than the corresponding phosphate esters. These results suggest that **IT6** is more resistant to phytase hydrolysis than **IP6**.

Solubility of IT6

It was previously observed that **IT6** was soluble in a simulated GI tract environment whereas **IP6** precipitated in the presence of the concentrations of $MgCl_2$ and $CaCl_2$ found in the intestinal lumen.[19] Cummer *et al.* found that the thiophosphate groups on **IT6** have a lower pK_a than the phosphates on **IP6**, resulting in **IT6** having a higher charge density at pH 7.4. They suggested that the greater charge density of **IT6** gave the compound a higher electroneutrality threshold point, thus enabling solubility at physiologically relevant concentrations of divalent cations. To explore this theory, we wanted to determine whether **IT6** was soluble in all concentrations of $CaCl_2$, or whether a critical point for precipitation existed for **IT6** that was previously untested. We determined the concentration of soluble **IP6** and **IT6** when 4 mM of each ligand was combined with a serial dilution of $CaCl_2$ at the physiological pH 7.4 in the presence of TMP. Phosphorus NMR with proton coupling (^{31}P–{^{1}H} NMR) was run on the supernatant to determine the concentration of soluble ligand, and these values were plotted against the corresponding $CaCl_2$ concentration (Fig. 3A and B). We found that **IT6** does precipitate out of solution in the presence of $CaCl_2$, although it requires a much higher concentration than **IP6** (32 mM *vs.* 4 mM $CaCl_2$). Therefore, **IT6** is soluble in physiologically relevant concentrations of $CaCl_2$, as its precipitation threshold is outside the physiologically relevant range (1–10 mM).[33]

While performing the quantification of soluble **IT6** *via* ^{31}P–{^{1}H} NMR an unexpected observation was made. Two species of **IT6** were detected, one that corresponded with the ^{31}P–{^{1}H} NMR spectrum of deprotonated **IT6**,[19] and another that only appeared in the presence of $CaCl_2$. The second species increased in quantity as $CaCl_2$ was added to the sample, and this change was inversely proportional to that of the deprotonated **IT6** species, indicating that the second species was a by-product of calcium chelating to **IT6** (**IT6**·xCa^{2+}, Fig. 3C). This observation was not apparent for **IP6** bound to Ca^{2+}. These results suggest that Ca^{2+} first chelates to **IT6**, forming a complexed species, which then precipitates out of solution, as the concentration of soluble **IT6** only decreased after all of the deprotonated **IT6** was converted into the complexed form as observed by ^{31}P–{^{1}H} NMR. Of note, **IP6** has been found to undergo a ring-flip with five axial substituents in the presence of certain environmental factors, such as metal cation composition.[34] However, ^{13}C NMR of the **IT6** samples indicated that the putative **IT6**·xCa^{2+} species was not a by-product of a "flipped" conformation (Fig. S4, ESI†).

Finally, the presence of precipitate formation was confirmed by dynamic light scattering (DLS, Fig. 3D and E). The mean diameter of **IP6** and **IT6** in solution at pH 7.4 increased as the amount of soluble ligand decreased. The size of the precipitate positively correlated with increased concentrations of $CaCl_2$. Collectively, these results support the theory that the increased charge density of **IT6** requires a greater concentration of $CaCl_2$ to cause charge neutralization of the compound, which initiates precipitation.

Characterizing the binding interaction between IT6 and AvrA

Cummer *et al.* previously found that **IT6** had a higher binding affinity for the *Clostridioides difficile* toxin B (TcdB) cysteine protease domain (CPD) allosteric binding site than its natural co-factor **IP6**. They suggested that this was due to the increased net charge density of **IT6** as the target binding site was electropositive, thus enhancing the electrochemical interaction.[19] Here we aimed to determine whether this property could be ascertained for other **IP6**-dependent virulence factors.

AvrA is an *S. typhimurium* effector protein, which suppresses c-JUN N-terminal kinase (JNK) signalling in mammals

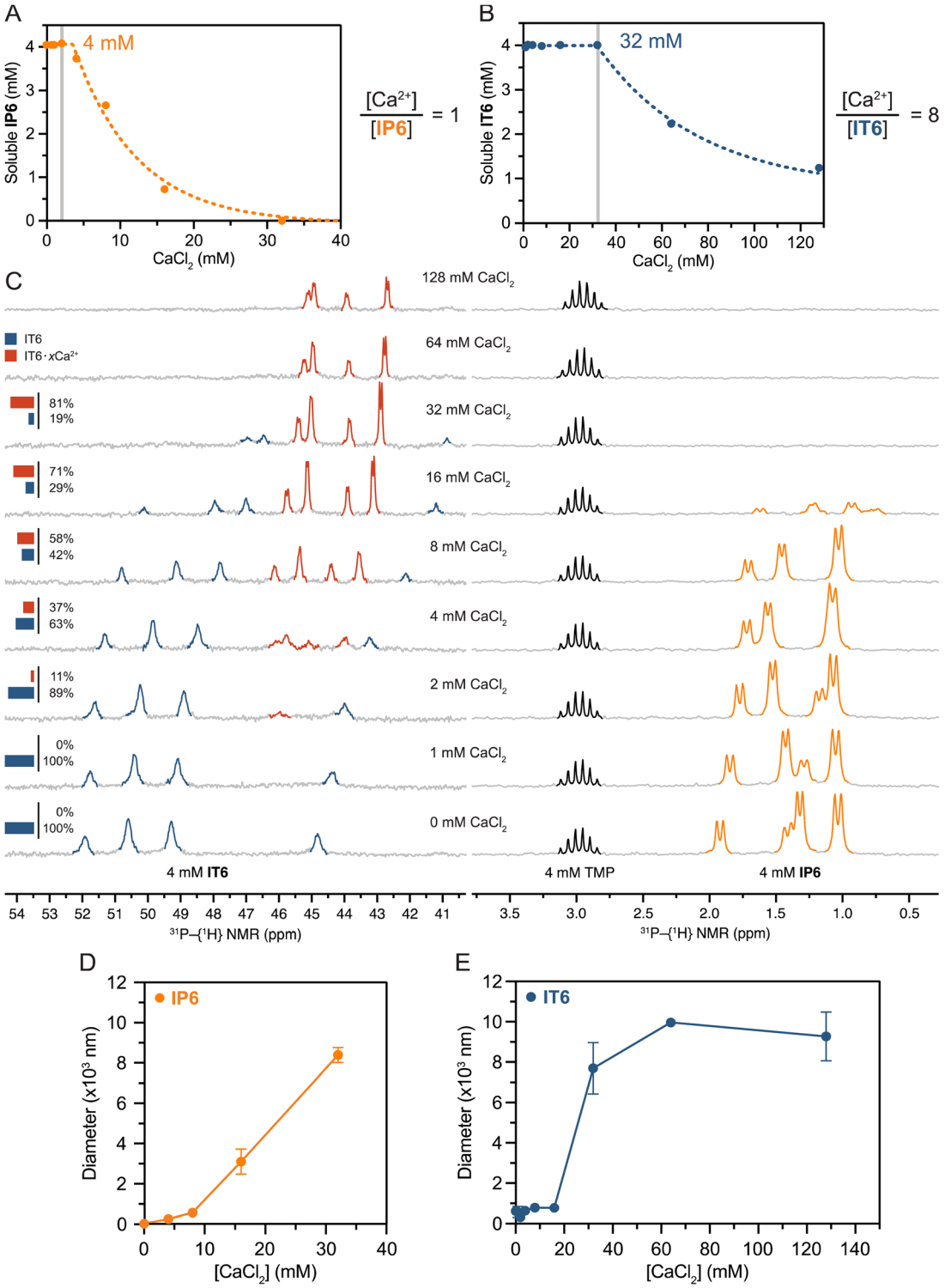

Fig. 3 Solubility differences between **IP6** and **IT6**. (A) Amount of soluble **IP6** and (B) **IT6** at pH 7.4 in the presence of an increasing concentration of $CaCl_2$. The amount of soluble ligand was calculated *via* $^{31}P–\{^1H\}$ NMR with TMP as an internal standard. Data are curve fit with a plateau followed by one phase decay in Prism 10. X_0 is noted with the gray line, and the corresponding ratio of $CaCl_2$ to ligand that induces precipitation is reported. (C) Stacked $^{31}P–\{^1H\}$ NMR spectra of **IT6** (blue/red) and **IP6** (orange) with varied concentrations of $CaCl_2$. The presence of $CaCl_2$ elicits the formation of an **IT6-Ca** complex (**IT6**·$x$$Ca^{2+}$, red) with a unique $^{31}P–\{^1H\}$ NMR profile. The percentage of **IT6** and **IT6**·$x$$Ca^{2+}$ was calculated for each $^{31}P–\{^1H\}$ NMR spectrum. The average particle diameter (nm) of 4 mM **IP6** (D) and **IT6** (E) at pH 7.4 was calculated at various concentrations of $CaCl_2$ *via* DLS.

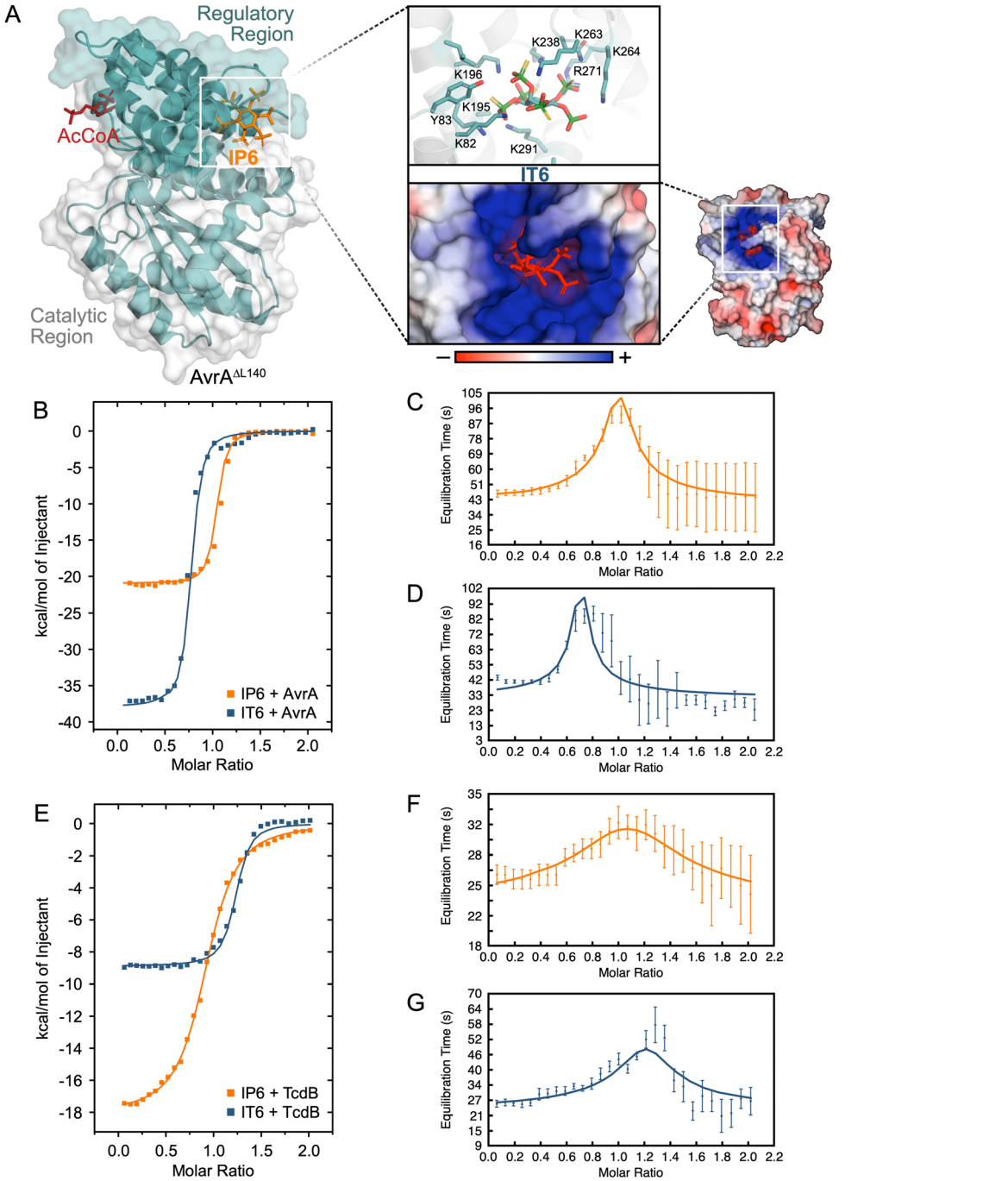

Fig. 4 Characterization of the binding interaction between bacterial virulence factors and **IP6** *versus* **IT6**. (A) Crystal structure of AvrA$^{\Delta L140}$ bound to **IP6** and AcCoA (PDB 6BE0).[10] **IP6** binds to an allosteric binding site in the regulatory region of AvrA that controls the formation of the AcCoA active site. **IP6** binds to the very positively charged allosteric binding site. Inset: Docking experiments show that **IT6** binds to the same positively charged pocket.[37,38] The binding interaction between AvrA and TcdB CPD with **IP6** and **IT6** was determined *via* ITC. The resultant thermograms (B) and (E) and the equilibration time curves (C) and (D) are shown for **IP6**/**IT6** with AvrA and **IP6**/**IT6** with TcdB CPD (F) and (G).

through acetylation of mitogen activated receptor kinases 4 and 7 (MKK4/7). Acetylation of MKK4/7 is suspected to reduce the upregulation of the host inflammatory response upon bacterial infection.[35] The acetyltransferase has two closely associated domains: a regulatory region and a catalytic region. The regulatory region mediates binding of the cofactors **IP6** and acetyl CoA (AcCoA), and the catalytic region acetylates the bound substrate (Fig. 4A).[10] Binding of **IP6** induces structural changes that form the substrate binding sites.[36] The **IP6** allosteric binding site contains many basic amino acids that are positively charged at a neutral pH and are stabilized by the negatively charged co-factor, as observed for TcdB CPD.

We wanted to determine whether **IT6** had a stronger affinity to AvrA than **IP6**. The equilibrium dissociation constants (K_d) of

IP6 and **IT6** were determined *via* isothermal calorimetry (ITC) (Fig. 4B and E). The K_d of **IT6** was 2.5-fold lower than that of **IP6** for AvrA, which was the same fold-change observed for TcdB CPD (Table 1). Of note, the reported K_d of AvrA with **IP6** was significantly lower than previously described (139 nM *versus* 5.18 μM).[10] We suspect that this discrepancy arose from the use of different sources of **IP6**. **IP6** needs to be stored in dry conditions, because if water of crystallization is present in the industrial preparation, **IP6** is susceptible to hydrolysis (Fig. S6, ESI†). If **IP6** was in fact a lower phosphorylated species, the resultant decreased net charge would explain the discrepancy with the previously reported K_d.

To look beyond the strength of interaction we can also investigate the durability of the binary ligand–protein complex. The improved electrostatic interaction between **IT6** and AvrA/TcdB CPD is a molecular determinant of the dissociation rate constant (k_{off}), and this dissociation process defines the drug-target residence time (τ_R).[39] We determined the k_{off} of the interactions *via* the kinetic ITC (kinITC) methodology utilized by the AFFINImeter software.[40,41] The equilibration time curves (ETC, Fig. 4C, D, F and G) were curve fit with a one-site model, and the goodness of fit for each measurement had a χ^2 below 2, indicating a strong fit. The ETC's gave a k_{off} measurement from the ITC raw data (Table 1). The lower k_{off} of **IT6** indicated that it had a longer-lived ligand-target complex with both AvrA and TcdB CPD than **IP6** (AvrA τ_R = 14.4, 9.7 min; TcdB CPD τ_R = 2.4, 0.4 min). Therefore, the increased charge density of **IT6** has an effect on the duration of target activation.

Stabilization of virulence factor effector proteins AvrA and VopA

Molecular dynamics simulations have been performed with both TcdB CPD and AvrA to show the structural modifications associated with **IP6** binding.[36,42] Finn *et al.* previously found that the conformational changes that accompany allosteric binding of **IP6** to the CPD on TcdB and toxin A (TcdA) were stabilized by a network of residue interactions, complementary to the unbound state residue network. The network involves electrostatic interactions between **IP6** and arginine and lysine residues in the allosteric binding site. In the **IP6**-bound conformation, an α-loop formed a 'lid' over the drug binding pocket, which acted to block the escape of the ligand, and a β-flap rotated ~90°, which resulted in the formation of the cysteine protease active site.[42] Similarly, Zhang *et al.* showed that binding of **IP6** to the allosteric binding site of AvrA induced structural changes that constrained two α-helices around **IP6**, which caused two β-strands in the regulatory domain to form the AcCoA and substrate binding sites.[36]

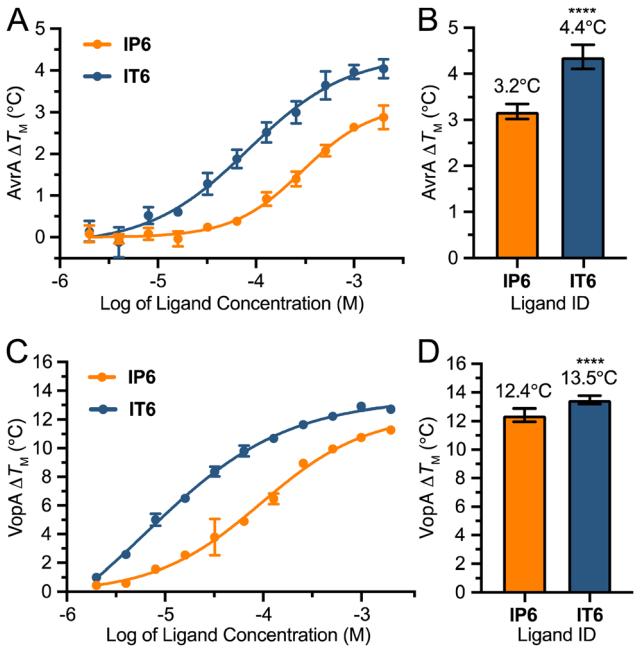

Fig. 5 Stabilization of the effector proteins AvrA and VopA. Dose–response curves for binding of **IP6** and **IT6** with AvrA (A) and VopA (C) and the corresponding temperature stabilization. Stabilization of AvrA and VopA was determined *via* DSF. The melting temperature (T_M) was determined for the proteins alone and in the presence of a serial dilution of **IP6** or **IT6**. The difference in melting temperature (ΔT_M) was then plotted and the data were fit with a nonlinear curve fit. Mean ± SD, n = 5. Maximal ΔT_M (°C) for **IP6** and **IT6** with AvrA (B) and VopA (D), as determined in (A) and (C), respectively. Mean ± SD, n = 5; independent t-test ****$p < 0.0001$.

The simple one-step binding/dissociation model that was used to describe the binding interaction between **IT6**/**IP6** and AvrA/TcdB-CPD may be insufficient to describe the interaction as the ligands induce conformational changes to the proteins. The conformational changes result in greater steric and electronic complementarity between the drug molecule and its binding site on the target and often greater occlusion from the solvent. The conformational changes associated with the transition from unbound to bound strengthen the binding of the ligand to its target and simultaneously decrease the rate of drug dissociation. Consequently, the τ_R of the drug–protein complex is considerably augmented. Therefore, understanding these changes by other biophysical methods can be of importance.

Here, we determined whether **IT6** was more capable than **IP6** at stabilizing AvrA and VopA, an ortholog of AvrA which is found in other enteric pathogens like *V. parahaemolyticus*.[43] To test this, we performed a differential scanning fluorimetry

Table 1 Enthalpy (ΔH), equilibrium dissociation constant (K_d), and rate of dissociation (k_{off}) with the equilibration time curve goodness of fit (χ^2) for **IP6** and **IT6** when bound to the bacterial virulence factors AvrA and TcdB CPD. Mean (SD)

Protein	Ligand	ΔH (kcal mol^{-1})	K_d (nM)	K_{off} (s^{-1})	χ^2
AvrA	**IP6**	−21.09 (0.12)	139.4 (16.4)	1.711×10^{-3} (1.71×10^{-4})	0.751
	IT6	−35.56 (0.32)	55.39 (15.4)	1.156×10^{-3} (1.91×10^{-4})	1.300
TcdB CPD	**IP6**	−22.94 (0.05)	1918 (34.6)	4.086×10^{-2} (5.52×10^{-3})	0.173
	IT6	−9.386 (0.14)	413.3 (57.8)	6.912×10^{-3} (7.22×10^{-4})	1.623

(DSF) experiment to determine the melting temperature (T_M) of AvrA and VopA alone and in the presence of serial dilutions of **IP6** and **IT6**. We then determined the change in T_M (ΔT_M) for each ligand concentration when compared to the T_M of AvrA or VopA alone (Fig. 5A and C, respectively). The sizable leftward shift in the dose response curve corresponding to **IT6** suggests that **IT6** may have an improved binding affinity when compared to **IP6**, and these results are corroborated by the ITC results for AvrA. However, when attempting to assess the binding affinity for VopA *via* ITC, we found that the protein was unstable in the absence of the ligand. VopA rapidly lost functionality or misfolded within hours after purification, leading to inconsistent ITC results.

To quantify the stabilizing effect of each ligand, we performed a nonlinear curve fit on the data to determine the maximal ΔT_M for **IP6** and **IT6** on AvrA and VopA (Fig. 5B and D, respectively). We found that **IT6** had a significantly higher ΔT_M than **IP6** when bound to both AvrA (3.2 °C *vs.* 4.4 °C) and VopA (12.4 °C *vs.* 13.5 °C), which reflected increased protein stabilization. Additionally, the enhanced stabilization of **IT6** over **IP6** was previously observed for TcdB CPD.[19] These results add further support to the theory that the improved charge density of the thiophosphate biomimetic, **IT6**, strengthens the electrostatic interaction with the **IP6**-dependent protein stabilizing the bound state, as observed here and previously with TcdB.[19]

Conclusions

Here, we propose **IT6** as an interesting biomimetic of **IP6** due to its suggested phytase stability, improved lipophilicity, solubility, and lower K_d and increased stabilization of the **IP6**-dependent proteins AvrA and TcdB-CPD. First, we found that **IT6** is resistant to phytase-4 degradation due to the thiophosphate phosphoryl group being less positively charged, making a nucleophilic attack unlikely, and circumventing the hydrolysis reaction. Second, we found that aprotic thiophosphates are less polar than phosphates, while protic thiophosphates have a greater charge density; these apparent contradictory properties have manifested themselves in multiple interesting capabilities. The decreased polarity of **IT6-Bn** in comparison with **IP6-Bn** has resulted in an improved lipophilicity of the functional group. Although this does not put **IT6-Bn**, or **IT6**, within the cell permeability range according to Lipinski's rules, other strategies have been developed to optimize the delivery of highly anionic compounds.[44] The increased charge density of thiophosphates at pH 7.4 has resulted in **IT6** solubility in physiological concentrations of divalent cations due to a higher concentration threshold for charge neutralization. The higher charge density has also improved the K_d, τ_R and stabilization of **IT6** for TcdB CPD, AvrA, and VopA in comparison with **IP6**. The unique properties of thiophosphate analogs suggest several potential practical applications that warrant further exploration. First, the drug-target τ_R model predicts that durable pharmacodynamics can be achieved by developing drug molecules with a long τ_R on their target.[39] These results suggest that further research should explore whether thiophosphate substitution of functional groups involved in electrostatic interactions improves the pharmacodynamic properties of other pharmaceuticals. Second, stabilization of **IP6**-dependent proteins by **IT6** might facilitate the formation of tractable crystal/ligand complexes for X-ray structural analysis.[44]

Abbreviations

AcCoA	Acetyl CoA
K_a	Association constant
clog P	Calculated log P
ΔT_M	Change in melting temperature
JNK	c-JUN N-terminal kinase
CPD	Cysteine protease domain
k_{off}	Dissociation rate constant
DLS	Dynamic light scattering
K_d	Equilibrium dissociation constant
GI	Gastrointestinal
IP6-Bn	*myo*-Inositol hexakis-dibenzylphosphate
IT6-Bn	*myo*-Inositol hexakis-dibenzylthiophosphate
HBB	Hydrogen bond basicity
ITC	Isothermal calorimetry
kinITC	Kinetic ITC
MKK4/7	Mitogen activated receptor kinases 4 and 7
T_M	Melting temperature
IP6	*myo*-Inositol hexakisphosphate
IT6	*myo*-Inositol hexakisthiophosphate
τ_R	Residence time
TcdB	Toxin B
TMP	Trimethyl phosphate.

Data availability

The data supporting this article have been included as part of the ESI.†

Conflicts of interest

The authors declare no conflicts of interest.

Acknowledgements

We would like to acknowledge Dr Kim Munro and the Centre for Structural Biology Research (CRBS), supported by the *Fond de Recherche du Québec–Santé* (FRQS), for use of the core facilities. NMR experiments were recorded at the Québec/Eastern Canada High Field NMR Facility, supported by the Canada Foundation for Innovation, McGill University Faculty of Science and Department of Chemistry. Mass Spectrometry and DLS experiments were performed by the McGill Chemistry Characterization facility. Funding for this project was provided by a Canadian Institutes of Health Research (CIHR) project grant (PJT-173262) to Dr Bastien Castagner and a Natural Science and Engineering Research council of Canada (NSERC) discovery grant (RGPIN-2020-04908) to Dr Castagner. Dr Castagner is a tier 2 Canada Research Chair (CRC) in Therapeutic Chemistry.

References

1 K. A. Woll and F. Van Petegem, *Physiol. Rev.*, 2022, **102**, 209–268.
2 A. J. López-Gambero, C. Sanjuan, P. J. Serrano-Castro, J. Suárez and F. Rodríguez de Fonseca, *Biomedicines*, 2020, **8**, 295.
3 B. Tu-Sekine and S. F. Kim, *Int. J. Mol. Sci.*, 2022, **23**, 6747.
4 J. Reineke, S. Tenzer, M. Rupnik, A. Koschinski, O. Hasselmayer, A. Schrattenholz, H. Schild and C. Von Eichel-Streiber, *Nature*, 2007, **446**, 415–419.
5 K. E. Orrell and R. A. Melnyk, *Microbiol. Mol. Biol. Rev.*, 2021, **85**, e0006421.
6 K. Prochazkova and K. J. F. Satchell, *J. Biol. Chem.*, 2008, **283**, 23656–23664.
7 A. Shen, P. J. Lupardus, V. E. Albrow, A. Guzzetta, J. C. Powers, K. C. Garcia and M. Bogyo, *Nat. Chem. Biol.*, 2009, **5**, 469–478.
8 R. A. Dick, K. K. Zadrozny, C. Xu, F. K. M. Schur, T. D. Lyddon, C. L. Ricana, J. M. Wagner, J. R. Perilla, B. K. Ganser-Pornillos, M. C. Johnson, O. Pornillos and V. M. Vogt, *Nature*, 2018, **560**, 509–512.
9 A. Sreelatha, C. Nolan, B. C. Park, K. Pawłowski, D. R. Tomchick and V. S. Tagliabracci, *J. Biol. Chem.*, 2020, **295**, 6214–6224.
10 J. M. Labriola, Y. Zhou and B. Nagar, *Biochemistry*, 2018, **57**, 4985–4996.
11 A. J. R. Costello, T. Glonek and T. C. Myers, *Carbohydr. Res.*, 1976, **46**, 159–171.
12 J. Torres, S. Domínguez, M. F. Cerdá, G. Obal, A. Mederos, R. F. Irvine, A. Díaz and C. Kremer, *J. Inorg. Biochem.*, 2005, **99**, 828–840.
13 S. R. Hull and R. Montgomery, *J. Agric. Food Chem.*, 1995, **43**, 1516–1523.
14 Y. Moritoh, S. Abe, H. Akiyama, A. Kobayashi, R. Koyama, R. Hara, S. Kasai and M. Watanabe, *Nat. Commun.*, 2021, **12**, 4847.
15 M. Nguyen Trung, S. Kieninger, Z. Fandi, D. Qiu, G. Liu, N. K. Mehendale, A. Saiardi, H. Jessen, B. Keller and D. Fiedler, *ACS Cent. Sci.*, 2022, **8**, 1683–1694.
16 A. S. M. G. M. Akond, H. Crawford, J. Berthold, Z. I. Talukder and K. Hossain, *Am. J. Food Technol.*, 2011, **6**, 235–243.
17 X. Li, Q. Wei, K. Zhao, W. Wang, B. Liu, W. Li and J. Wang, *ACS Sens.*, 2023, **8**, 4484–4493.
18 M. E. Ivarsson, E. Durantie, C. Huberli, S. Huwiler, C. Hegde, J. Friedman, F. Altamura, J. Lu, E. F. Verdu, P. Bercik, S. M. Logan, W. Chen, J.-C. Leroux and B. Castagner, *Cell Chem. Biol.*, 2019, **26**, 17–26.e13.
19 R. Cummer, F. Grosjean, R. Bolteau, S. E. Vasegh, S. Veyron, L. Keogh, J.-F. Trempe and B. Castagner, *J. Med. Chem.*, 2024, acs.jmedchem.4c01408.
20 A. Dostálková, F. Kaufman, I. Křížová, B. Vokatá, T. Ruml and M. Rumlová, *J. Virol.*, 2020, **94**, 10–1128.
21 A. Dostálková, B. Vokatá, F. Kaufman, P. Ulbrich, T. Ruml and M. Rumlová, *Viruses*, 2021, **13**, 129.
22 G. M. Blackbum, G. E. Taylor, G. R. J. Thatcher, M. Prescott and A. G. McLennan, *Nucleic Acids Res.*, 1987, **15**, 6991–7004.
23 G. M. Blackburn, P. R. Ashton, M.-J. Guo, M. Rogers, G. Taylor, A. Guranowski and D. Watts, *Heteroat. Chem.*, 1991, **2**, 163–170.
24 D. Lampe, C. Liu and B. V. L. Potter, *J. Med. Chem.*, 1994, **37**, 907–912.
25 A. M. Cooke, S. R. Nahorski and B. V. L. Potter, *FEBS Lett.*, 1989, **242**, 373–377.
26 Y. Xu, X. Liu and G. D. Prestwich, *Tetrahedron Lett.*, 2005, **46**, 8311–8314.
27 I. Columbus, L. Ghindes-Azaria, R. Chen, L. Yehezkel, O. Redy-Keisar, G. Fridkin, D. Amir, D. Marciano, E. Drug, E. Gershonov, Z. Klausner, S. Saphier, S. Elias, A. Pevzner, Y. Eichen, G. Parvari, B. Smolkin and Y. Zafrani, *J. Med. Chem.*, 2022, **65**, 8511–8524.
28 H.-J. Zhang, M. Ociepa, M. Nassir, B. Zheng, S. A. Lewicki, V. Salmaso, H. Baburi, J. Nagel, S. Mirza, B. Bueschbell, H. Al-Hroub, O. Perzanowska, Z. Lin, M. A. Schmidt, M. D. Eastgate, K. A. Jacobson, C. E. Müller, J. Kowalska, J. Jemielity and P. S. Baran, *Nat. Chem.*, 2024, **16**, 249–258.
29 B. Novotná, L. Vaneková, M. Zavřel, M. Buděšínský, M. Dejmek, M. Smola, O. Gutten, Z. A. Tehrani, M. Pimková Polidarová, A. Brázdová, R. Liboska, I. Štěpánek, Z. Vavřina, T. Jandušík, R. Nencka, L. Rulíšek, E. Bouřa, J. Brynda, O. Páv and G. Birkuš, *J. Med. Chem.*, 2019, **62**, 10676–10690.
30 D. Chen, N. Oezguen, P. Urvil, C. Ferguson, S. M. Dann and T. C. Savidge, *Sci. Adv.*, 2016, **2**, e1501240.
31 Degradation of Phytate by the 6-Phytase from Hafnia alvei: A Combined Structural and Solution Study|PLOS ONE, **https://journals.plos.org/plosone/article?id=10.1371/journal.pone.0065062**, accessed 11 July 2024.
32 P. H. Selle and V. Ravindran, *Anim. Feed Sci. Technol.*, 2007, **135**, 1–41.
33 J. G. J. Hoenderop, B. Nilius and R. J. M. Bindels, *Physiol. Rev.*, 2005, **85**, 373–422.
34 L. Kurz, P. Schmieder, N. Veiga and D. Fiedler, *Biomolecules*, 2023, **13**, 645.
35 R. M. Jones, H. Wu, C. Wentworth, L. Luo, L. Collier-Hyams and A. S. Neish, *Cell Host Microbe*, 2008, **3**, 233–244.
36 Z.-M. Zhang, K.-W. Ma, S. Yuan, Y. Luo, S. Jiang, E. Hawara, S. Pan, W. Ma and J. Song, *Nat. Struct. Mol. Biol.*, 2016, **23**, 847–852.
37 R. A. Friesner, J. L. Banks, R. B. Murphy, T. A. Halgren, J. J. Klicic, D. T. Mainz, M. P. Repasky, E. H. Knoll, M. Shelley, J. K. Perry, D. E. Shaw, P. Francis and P. S. Shenkin, *J. Med. Chem.*, 2004, **47**, 1739–1749.
38 R. A. Friesner, R. B. Murphy, M. P. Repasky, L. L. Frye, J. R. Greenwood, T. A. Halgren, P. C. Sanschagrin and D. T. Mainz, *J. Med. Chem.*, 2006, **49**, 6177–6196.
39 R. A. Copeland, D. L. Pompliano and T. D. Meek, *Nat. Rev. Drug Discovery*, 2006, **5**, 730–739.
40 D. Burnouf, E. Ennifar, S. Guedich, B. Puffer, G. Hoffmann, G. Bec, F. Disdier, M. Baltzinger and P. Dumas, *J. Am. Chem. Soc.*, 2012, **134**, 559–565.
41 Á. Piñeiro, E. Muñoz, J. Sabín, M. Costas, M. Bastos, A. Velázquez-Campoy, P. F. Garrido, P. Dumas, E. Ennifar, L. García-Río, J. Rial, D. Pérez, P. Fraga, A. Rodríguez and C. Cotelo, *Anal. Biochem.*, 2019, **577**, 117–134.

42 L. M. Finn, R. Cummer, B. Castagner and B. G. Keller, *Proc. Natl. Acad. Sci. U. S. A.*, 2025, **122**, e2419263122.
43 J. E. Trosky, S. Mukherjee, D. L. Burdette, M. Roberts, L. McCarter, R. M. Siegel and K. Orth, *J. Biol. Chem.*, 2004, **279**, 51953–51957.
44 I. Pavlovic, D. T. Thakor, J. R. Vargas, C. J. McKinlay, S. Hauke, P. Anstaett, R. C. Camuña, L. Bigler, G. Gasser, C. Schultz, P. A. Wender and H. J. Jessen, *Nat. Commun.*, 2016, **7**, 10622.